Chapter 14
Experimental Dynamic Characterization of Operating Wind Turbines with Anisotropic Rotor

Dmitri Tcherniak and Matthew S. Allen

Abstract The presented study concerns experimental dynamic identification of (slightly) anisotropic bladed rotors under operating conditions. Since systems with a rotating rotor do not fall into a category of time invariant system, a straightforward application of modal analysis is not valid. Under assumptions of linearity and constant angular speed, a system with rotating rotor can be considered as a linear periodically time variant (LPTV) system; dynamic identification of such systems require dedicated methods. The Harmonic OMA Time Domain (H-OMA-TD) method is one of very few techniques able to deal with anisotropic rotors. This study demonstrates the method on a simple six degrees-of-freedom mechanical system with a three-bladed rotor. It shows that the method is capable of identifying the phenomena specific for anisotropic rotors. The technique is compared with another technique, multiblade coordinate (MBC) transformation, and the advantages of H-OMA-TD become apparent when the rotor is anisotropic. Finally, the method is demonstrated on data measured on a real Vestas V27 wind turbine and data obtain via HAWC2 simulations of the same wind turbine.

Keywords Linear periodic time variant system • LPTV • Dynamic identification • Wind turbine

14.1 Introduction

The presented paper concerns the methods for experimental identification of bladed rotors with slight anisotropy. In industry, such methods are valuable means for investigation of dynamics of operating wind turbines. The current tendency in wind energy can be characterized by bigger wind turbines, greater wind loads (especially for offshore machines), lighter structures and longer lifetime. All these require the detailed understanding of wind turbine dynamic behavior while operating, and demand proper experimental techniques for their dynamic identification.

While a standstill wind turbine can be considered as a linear time-invariant (LTI) system, an operating wind turbine certainly does not fall into this category. It is easy to demonstrate that the mass, stiffness, damping and gyroscopic matrices are dependent on rotor azimuth angle. Still assuming the linearity and constant rotor angular speed, one can categorize such a system as Linear Periodic Time-variant (LPTV, or LTP) system. Then, instead of well-established tools suitable for LTI systems, such as modal analysis and experimental techniques such as EMA and OMA, one needs to employ tools that are more advanced.

In most of the practical cases, the rotor of a wind turbine is not completely isotropic. Despite the efforts of wind turbine manufactures, the rotor blades are never identical; there is some degree of rotor anisotropy even for a newly erected wind turbine. During the lifetime, the degree of anisotropy can increase temporarily or permanently. The former can happen e.g. due to ice formation on one of the blades, the latter—due to damage or loss of structural integrity of one of the blades, failure of the pitch mechanism or blade attachment to the hub. Such rotor anisotropy is considered as an "off-optimum situation" and shall be detected and avoided, if possible. Understanding and being able to characterize the differences in the dynamics between the isotropic and anisotropic rotors can apparently help in the abovementioned scenarios. Thus, one needs a proper tool for experimental dynamic characterization of operating wind turbine whose rotor might be slightly anisotropic.

D. Tcherniak (✉)
Brüel & Kjær Sound & Vibration Measurement, Skodsborgvej 307, Nærum 2850, Denmark
e-mail: dmitri.tcherniak@bksv.com

M.S. Allen
Department of Engineering Physics, University of Wisconsin-Madison, 535 Engineering Research Building, 1500 Eng. Drive, Madison, WI 53706, USA
e-mail: msallen@engr.wisc.edu

S. Pakzad, C. Juan (eds.), *Dynamics of Civil Structures, Volume 2*, Conference Proceedings of the Society for Experimental Mechanics Series, DOI 10.1007/978-3-319-29751-4_14

The tools allowing experimental dynamic characterization of LPTV systems are very limited: one can name MBC transformation adopted to experimental identification [1], the extension of stochastic subspace identification (SSI) to LPTV systems based on angular resampling [2] and harmonic power spectra (HPS) based methods [3]. The MBC transformation method assumes that the rotor is isotropic, it was demonstrated that application of this method to a system with an anisotropic rotor leads to incorrect results [4]. The method based on resampling was designed for systems with fast-rotating rotors such as helicopter, and its application to wind turbine data was not very successful [5]. For today, the HPS-based methods seem to be most suitable for wind turbine applications. Originally implemented in frequency domain (referred as H-OMA-FD) [6], the method was successfully applied to simulated wind turbine data (with isotropic rotor) [3] and to the data measured on real Vestas V27 wind turbine [7]. The time domain implementation of the method (referred as H-OMA-TD) was suggested by the authors in [8], and in [9] it was applied to the data measured on Vestas V27 wind turbine.

Because system identification methods are only now emerging for LPTV systems, there are still very few studies that treat turbines with blade anisotropy, and so it is challenging to understand how the results relate to the turbine's performance. The present study focuses on the effects of rotor anisotropy and investigates how these effects can be identified from experimentally obtained data using H-OMA-TD method. The paper is built as follows: Sect. 14.2 explains what we understand under *dynamic characterization of LPTV systems*; Sect. 14.3 briefs the reader for MBC- and HPS-based methods and explains why MBC transformation is not suitable for anisotropic systems. Section 14.4 demonstrates the H-OMA-TD method in application to systems with anisotropic bladed rotors: first we consider a simple six degree-of-freedom and then demonstrate the method on simulated and measured data from a Vestas V27 wind turbine.

14.2 Theoretical Background

Consider a LTI system governed by equation

$$\mathbf{M}\ddot{\mathbf{y}}(t) + \mathbf{C}\dot{\mathbf{y}}(t) + \mathbf{K}\mathbf{y}(t) = \mathbf{0} \tag{14.1}$$

where $\mathbf{M}, \mathbf{C}, \mathbf{K} \in R^{N\times N}$ are mass, damping and stiffness matrices respectively and vector $\mathbf{y}(t) \in R^N$ is the displacements of system's N degrees of freedom over time t. The solution to (14.1) can be presented as modal decomposition

$$\mathbf{y}(t) = \sum_{r=1}^{N} b_r\, \boldsymbol{\phi}_r e^{\lambda_r t} \tag{14.2}$$

where the mode shape $\boldsymbol{\phi}_r \in \mathbb{C}^N$ and eigenvalue $\lambda_r \in \mathbb{C}$ constitute the modal parameters for the rth mode and $b_r \in \mathbb{C}$ is the mode participation factor, which depends on the system initial conditions. Since one can completely characterize all of the possible dynamic responses of this system in terms of its modal parameters, finding them is often called system's *dynamic characterization*. When the equation of motion is known, modal parameters can be found via eigenvalue analysis, e.g. [10]. In case when the equation of motion is unknown, we use experimental or operational modal analysis (EMA or OMA).

The mass, damping/gyroscopic and stiffness matrices of a system *with rotating rotor* depend on rotor position (azimuth angle θ)

$$\mathbf{M}(\theta(t))\ \ddot{\mathbf{y}}(t) + \mathbf{G}(\theta(t))\,\dot{\mathbf{y}}(t) + \mathbf{K}(\theta(t))\,\mathbf{y}(t) = \mathbf{0}. \tag{14.3}$$

Under the assumption that the rotor angular speed $\Omega = const$, thus $\theta(t) = \Omega t$, the matrices become time-periodic $\mathbf{M}(t+T) = \mathbf{M}(t), \mathbf{G}(t+T) = \mathbf{G}(t), \mathbf{K}(t+T) = \mathbf{K}(t)$ with period $T = 2\pi/\Omega$. We refer to such a system as an LPTV or LTP system.

The main assumption of modal analysis, that the system under test is time invariant, is violated here. It means that generally modal analysis and modal decomposition are not applicable to LPTV systems. However, *Floquet theory* suggests a decomposition, similar to (14.2) but involving T-periodic mode shapes $\mathbf{u}_r(t)$

$$\mathbf{y}(t) = \sum_{r=1}^{N} b_r \mathbf{u}_r(t) e^{\lambda_r t} \tag{14.4}$$

The periodic mode shapes can be expanded using Fourier transform

$$\mathbf{u}_r(t) = \sum_{n=-\infty}^{+\infty} \mathbf{C}_{r,n} e^{jn\Omega t} \tag{14.5}$$

and finally, the solution to (14.3) can be written as a modal superposition of sums of the harmonic components:

$$\mathbf{y}(t) = \sum_{r=1}^{N} b_r \sum_{n=-\infty}^{+\infty} \mathbf{C}_{r,n} e^{(\lambda_r + jn\Omega)t} \tag{14.6}$$

Thus, when saying *dynamic characterization of an LPTV system*, we mean finding its *Floquet exponents* $\lambda_r \in \mathbb{C}$ and the *Fourier coefficients* $\mathbf{C}_{r,n} \in \mathbb{C}^N$. Comparing (14.2) and (14.6), one can see many similarities: in both cases the solution is presented as modal superposition; the Floquet exponents are similar to the eigenvalues of the LTI system; they combine its natural frequency (the imaginary part) and damping (the real part). The Fourier coefficients can be thought as an infinite set of complex vectors, which together represent a periodic mode shape of the LPTV system, and thus they resemble the mode shape of the LTI system $\boldsymbol{\phi}_r$.

If the equation of motion is known, the Floquet exponents and Fourier coefficients can be found via *Floquet analysis* (for small number of DOFs) or *implicit Floquet analysis* (for great DOFs number), see [11], Table 3.1. To *experimentally characterize* an LPTV system, dedicated methods are needed, as will be considered the next section.

14.3 Experimental Techniques for LPTV Systems

There is a very limited set of tools applicable to experimental identification of LPTV systems. Here we briefly introduce multiblade coordinate (MBC) transformation and harmonic power spectra (HPS) based methods.

14.3.1 Multiblade Coordinate (MBC) Transformation

MBC transformation in application to wind turbines was introduced by Hansen, and its detailed description can be found in [12, 13]. The idea of the method lies in special coordinate transformation known as a *multiblade coordinate* or *Coleman* transformation. For a three-bladed rotor, the forward MBC transformation

$$a_{0,k}(t) = \frac{1}{3}\sum_{i=1}^{3} q_{i,k}(t), \quad a_{1,k}(t) = \frac{2}{3}\sum_{i=1}^{3} q_{i,k}(t)\cos(\theta_i(t)), \quad b_{1,k}(t) = \frac{2}{3}\sum_{i=1}^{3} q_{i,k}(t)\sin(\theta_i(t)) \tag{14.7}$$

converts the set of three coordinates $q_{i,k}$ measured at kth DOF of blade no. $i = 1, 2, 3$ into a set of three *multiblade coordinates* $a_{0,k}$, $a_{1,k}$ and $b_{1,k}$. The transformation uses $\theta_i(t)$, which is the azimuth of the ith blade.

Typically, vector $\mathbf{y}(t)$ is a mixture of the coordinates measured on the rotating rotor ($q_{i,k}$) and those measured on not rotating substructures, e.g. on the tower and nacelle (s_l):

$$\mathbf{y}(t) = \{\ldots, q_{1,k}(t), q_{1,k}(t), q_{3,k}(t), \ldots, s_1(t), \ldots, s_L(t)\}^T. \tag{14.8}$$

By substituting the coordinates measured on the rotating frame by the corresponding multiblade coordinates, it can be shown that, under the assumptions outlined below, the LPTV system transforms into an LTI system. Then, the conventional eigenvalue analysis can be performed on the obtained LTI system, resulting in eigenvalues and eigenvectors in multiblade coordinates. Finally, the eigenvectors can be converted back into the physical coordinates using the *backward multiblade coordinate* transformation

$$q_{i,k}(t) = a_{0,k}(t) + a_{1,k}(t)\cos(\theta_i(t)) + b_{1,k}(t)\ \sin(\theta_i(t)). \tag{14.9}$$

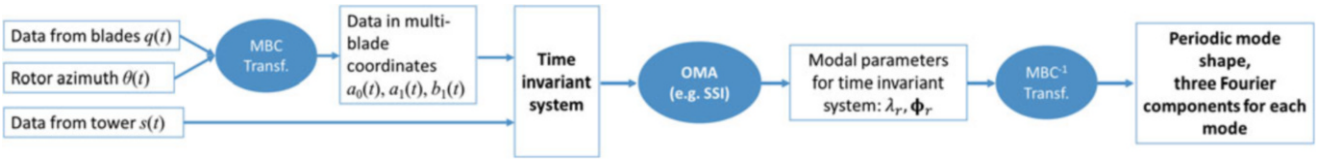

Fig. 14.1 Adaptation of MBC transformation to OMA

It is important to note that MBC transformation converts the LPTV system into the LTI system if the following assumptions fulfill:

1. The rotor is isotropic, i.e. the blades are identical and attached identically to the hub;
2. There is no gravity (for horizontal axis wind turbine, this condition can be relaxed for out-of-plane rotor modes since the out-of-plane blade motion is roughly perpendicular to the vector of gravity).

In [1], the MBC transformation was adopted to experimental system identification, combining the MBC transformation with Operational Modal Analysis (OMA); the flow is shown schematically in Fig. 14.1. The approach was demonstrated on simulated data [1] and on the data measured on operating Vestas V27 wind turbine [4, 7].

Applying the backward MBC transformation (14.9) to the mode shapes of the time invariant system, one can show that in physical coordinates the mode shape becomes periodic

$$\begin{aligned} u_{i,k}(t) = A_{0,k}\sin\left(\omega_r t + \varphi_{0,k}\right) + A_{BW,k}\sin\left(\left(\omega_r + \Omega\right)t + \tfrac{2\pi(i-1)}{3} + \varphi_{BW,k}\right) \\ + A_{FW,k}\ \sin\left(\left(\omega_r - \Omega\right)t - \tfrac{2\pi(i-1)}{3} + \varphi_{FW,k}\right) \end{aligned} \tag{14.10}$$

where $\omega_r = Im\left(\lambda_r\right)$ is the natural frequency of the rth mode of the time invariant system.

Analyzing (14.10), one can note that:

1. The method produces time periodic mode shapes, which always consist of three components.
2. The three components oscillate at frequencies ω_r, $\omega_r + \Omega$ and $\omega_r - \Omega$.
3. All three blades have identical oscillation magnitudes.
4. The phase between the blades is 0 for the first component (thus it is called *collective* component), $-120°$ for the second (*backward whirling* component) and $+120°$ for the third (*forward whirling* component).
   The last two properties can be described as a mode shape *symmetry*. That is, MBC transformation *always* produces modes with symmetric mode shapes.
5. The coordinates measured on the not rotating parts always have only a single component, namely at frequency ω_r.

Drawing the analogy with the Floquet theory, one can notice that (14.10) is a truncated version of (14.5), where $n = -1$, 0, 1; λ_r and $\lambda_r \pm \Omega$ are the three Floquet exponents and the pairs $(A_{X,k}, \varphi_{X,k})$ can be considered as kth element in the Fourier coefficient vector.

It becomes obvious, that application of the MBC transformation to the data measured on anisotropic rotor will lead to erroneous results. The effects of anisotropy, such as modes' asymmetry, will be smeared out by the MBC transformation and cannot be correctly identified. Analysis of such a possible erroneous interpretation can be found in [4].

14.3.2 Harmonic OMA (Frequency Domain) or H-OMA-FD

Allen et al. [3] suggested a framework for experimental identification of LPTV systems. The framework is based on the Floquet theory [14] and on the concept of harmonic transfer functions introduced by Wereley [15]. The method does not assume rotor isotropy, and thus directly suitable for analyzing anisotropic rotors. The detailed description of the approach can be found in [3], below we only present its main steps, which are also outlined in Fig. 14.2.

The core of the method is the *modulation* of the response signals using the phasors rotating with the fundamental circular frequency Ω and its integer multipliers

$$\mathbf{y}_m(t) = \mathbf{y}(t)e^{-jm\Omega t}, \quad m = -M \ldots M, m \in \mathbb{Z}. \tag{14.11}$$

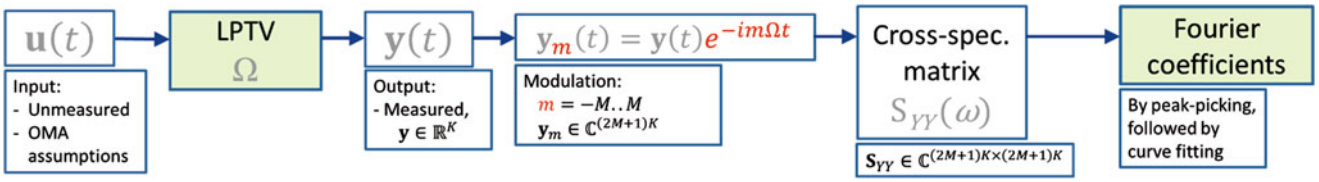

Fig. 14.2 Steps of H-OMA-FD method

Here $\mathbf{y}(t)$ is a vector of measured responses, $\mathbf{y}(t) \in \mathbb{R}^K$, see (14.8). The resulting vector consists of $(2M+1)K$ complex time histories, $\mathbf{y}_m(t) \in \mathbb{C}^{(2M+1)K}$. The next step of the method is the calculation of the harmonic power spectra (HPS) matrix between the modulated signals:

$$\mathbf{S}_{YY}(\omega) = \mathrm{E}\left\langle \mathbf{y}_{\boldsymbol{m}}(\omega)\, \mathbf{y}_{\boldsymbol{m}}(\omega)^H \right\rangle, \tag{14.12}$$

where $\mathrm{E}\langle \ldots \rangle$ is mathematical expectation, $(\ldots)^H$ is Hermitian transpose. Note that the resulting matrix is defined in the frequency domain. The theory in [3] states that the HPS matrix can be presented in terms of modes of the LPTV system. Preserving only dominant terms, [3] proves that the HPS matrix can be decomposed as:

$$\mathbf{S}_{YY}(\omega) \approx \sum_{r=1}^{N} \sum_{n=-\infty}^{\infty} \frac{\mathbf{C}_{n,l} \mathbf{W}(\omega)\, \mathbf{C}_{n,l}^H}{(j\omega - (\lambda_r - jn\Omega))\,(j\omega - (\lambda_r - jn\Omega))^H} \tag{14.13}$$

where λ_r are the Floquet exponents, $\mathbf{C}_{r,n}$ are the Fourier coefficients and N is the number of modes. $\mathbf{W}(\omega)$ describes the input spectrum. Under the standard OMA assumptions regarding the excitation, $\mathbf{W}(\omega)$ becomes an identity matrix.

Finally, the Floquet exponents and Fourier coefficients are extracted from the HPS matrix. This can be done by employing one of the conventional frequency domain methods known from classical modal analysis.

The method operates in frequency domain, and we refer to it as H-OMA-FD method. The method was successfully applied to simulated data from randomly excited Mathieu oscillator and simulated data from an operating wind turbine [3] and to the measured data from an operating Vestas V27 wind turbine [7].

14.3.3 Harmonic OMA (Time Domain) or H-OMA-TD

The recent advances in OMA, especially the improvements of the time domain OMA algorithms such as SSI, make it attractive to replace the curve fitting part of H-OMA-FD by OMA SSI. The adaptation of H-OMA-FD method to OMA SSI was suggested and explained in [8]. In analogy to H-OMA-FD, we refer this extension as Harmonic OMA Time Domain (H-OMA-TD). Below the main steps of the method are presented (and outlined in Fig. 14.3).

The first step of the two algorithms is the same: the measured signals are modulated using the phasor rotating at the rotor speed and its integer multipliers (14.11). In real applications the rotor speed can slightly vary; in this case it is advantageous to measure and use the rotor azimuth angle $\theta(t)$: $\mathbf{y}_m(t) = \mathbf{y}(t)e^{-jm\theta(t)}$. The resulting time histories are complex. To be able utilizing commercial OMA implementations (e.g. SVS ARTeMIS or B&K OMA software Type 7760), one needs to make the time histories real, still conserving the important dynamic information contained in the modulation. Two approaches to convert the modulated signals to real time histories are suggested in [8]; if the OMA implementation allows using complex time histories, this step can be omitted. The "Special data assignment to geometry" step is illustrated in Fig. 14.4, it serves to ease the interpretation of the results. It consists of creating $2M$ "clones" of the original test object geometry and assigning the modulated data to the clones. Finally, the modulated signals are processed by the OMA algorithm, resulting in modal parameters, which can be interpreted as Floquet exponents and the Fourier coefficients; the latter can be animated to visualize each component of the mode shapes. The interpretation of the results is explained in detail in [8].

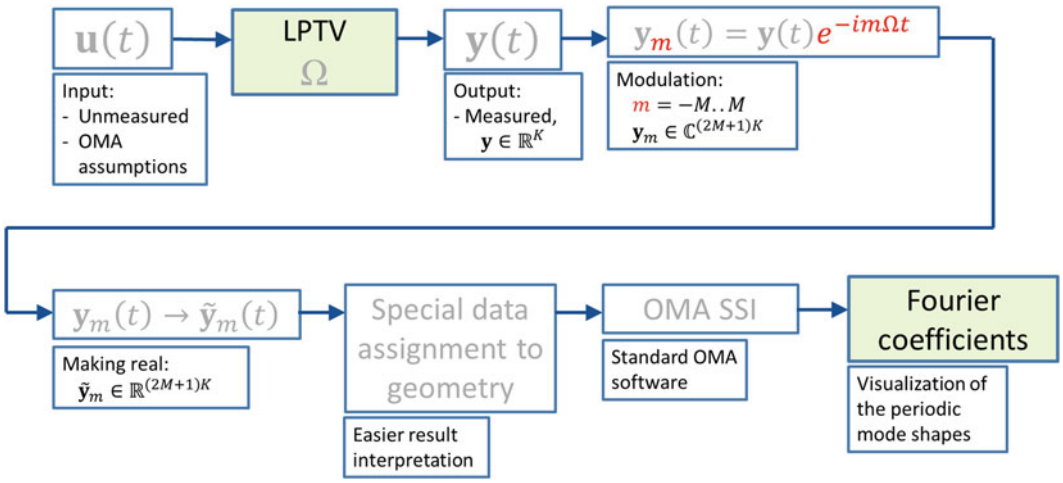

Fig. 14.3 Steps of H-OMA-TD method

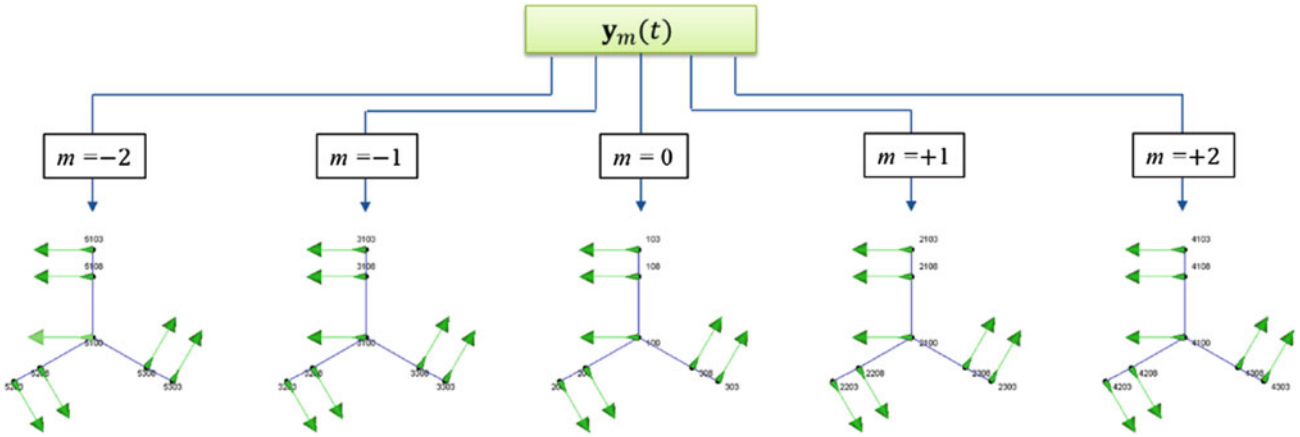

Fig. 14.4 Special data assignment to the geometry

14.3.4 Selection of M

Expression (14.5) expands the periodic mode shape using an infinite number of Fourier components. This is not feasible in practice, and one has to truncate the series:

$$\mathbf{u}_r(t) \approx \sum_{n=-M}^{+M} \mathbf{C}_{r,n} e^{jn\Omega t} \tag{14.14}$$

In the experimental interpretation of the HPS-based method, this corresponds to the selection of M in (14.11). Selecting the value of M, one can take into account the following considerations: As it follows from the MBC transformation (see Sect. 14.3.1), a three bladed isotropic rotor in the absence of gravity requires exactly three Fourier components, thus setting $M = 1$ is sufficient to describe such a rotor. Gravity and anisotropy will require more Fourier components. From authors experience, selecting $M = 2$ or $M = 3$ is sufficient for most wind turbine related cases, when there are three blades and the rotor anisotropy is not too large.

14.4 Application to Anisotropic Rotor

14.4.1 Application to a Simple Six Degree-of-Freedom System

In order to validate the method, let us consider a simple six degree-of-freedom system representing a three-bladed rotor mounted on a supporting structure (Fig. 14.5). The rotor is attached to a mass, which is supported in vertical and horizontal directions by two springs representing the bending and axial stiffness of the tower. Each rotor blade is constructed from two rigid arms, connected by a hinge with an angular spring modelling blade stiffness. The lumped mass at the end of the blade represents blade's mass. The system can model the blade dynamics in the rotor plane and the associated motion of the supporting mass and the "drive train". The same model was considered in [16], where the details are provided. The parameters of the model were selected to represent a 10 MW wind turbine prototype whose rotor rotates at 9.6 rpm (the fundamental frequency is 0.16 Hz).

The system can be fully described by the set of coordinates $\mathbf{y} = \{x_C, y_C, \phi_1, \phi_2, \phi_3, \psi\}^T$, where x_C, y_C are the coordinates of the mass C, angles ϕ_1, ϕ_2, ϕ_3 describe the angular displacements in the hinges and angle ψ is the angular deformation of the flexible "drive train".

Knowing the parameters of the system, the equations of motion can be readily defined, and the Floquet analysis can provide the Floquet exponents and Fourier coefficients for all six modes of the structure. The application of Floquet analysis to the system is straightforward though cumbersome; it is described in details in [16] and omitted here. The results of the Floquet analysis are used as a baseline for the H-OMA-TD method validation.

The validation is conducted via a simulated experiment: the system is subjected to random broadband excitation applied to the supporting mass and to the tips of the blades; and its response is simulated via time domain integration of the equations of motion using fourth order *Runge-Kutta* method. The obtained time histories become an input to the H-OMA-TD algorithm, which identifies the modal parameters (Floquet exponents and Fourier coefficients) of the turbine. These are then compared with the analytically obtained ones for isotropic and anisotropic rotors. The rotor anisotropy is modelled as a 3 % reduction of the stiffness of blade #3: $k_3 = 0.97k_1$.

The focus of the paper is to assess the ability of H-OMA-TD to catch the dynamic features intrinsic to an anisotropic rotor, thus we chose the following validation strategy: First we compare the results of Floquet analysis for an isotropic rotor, with that for anisotropic rotors, with anisotropy due to gravity and due to differing blade stiffness. This reveals features in the Floquet exponents and Fourier coefficients that are indicative of anisotropy. Then, we apply *H-OMA-TD* to the simulated isotropic and anisotropic rotors to see whether one can detect the features characteristic to anisotropic rotor from experimental data.

Figure 14.6 shows three rotor related modes, in industry these modes are traditionally called the backward whirling (BW) mode, forward whirling (FW) mode and collective mode. Three other modes (two tower related and one related to the drive-train) are not shown. Each mode consists of a number of Fourier components, oscillating at frequencies separated by Ω. The component with the biggest magnitude is placed in the center of the plot. One can see that the magnitude of the Fourier coefficients quickly decreases when moving away from the central component, meaning that only a small number of Fourier coefficients is required to describe modes' periodicity. However, one has to be careful when selecting this number since it will increase for rotors with higher degree of anisotropy.

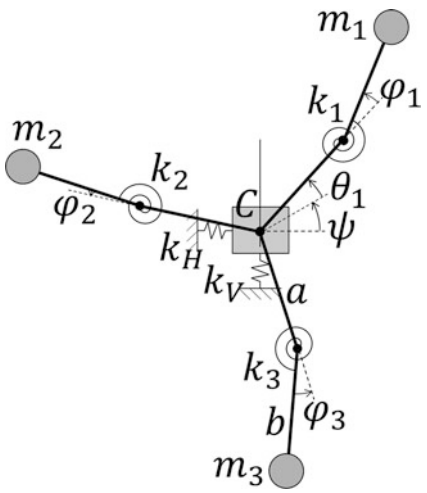

Fig. 14.5 Simplified three-bladed rotor system

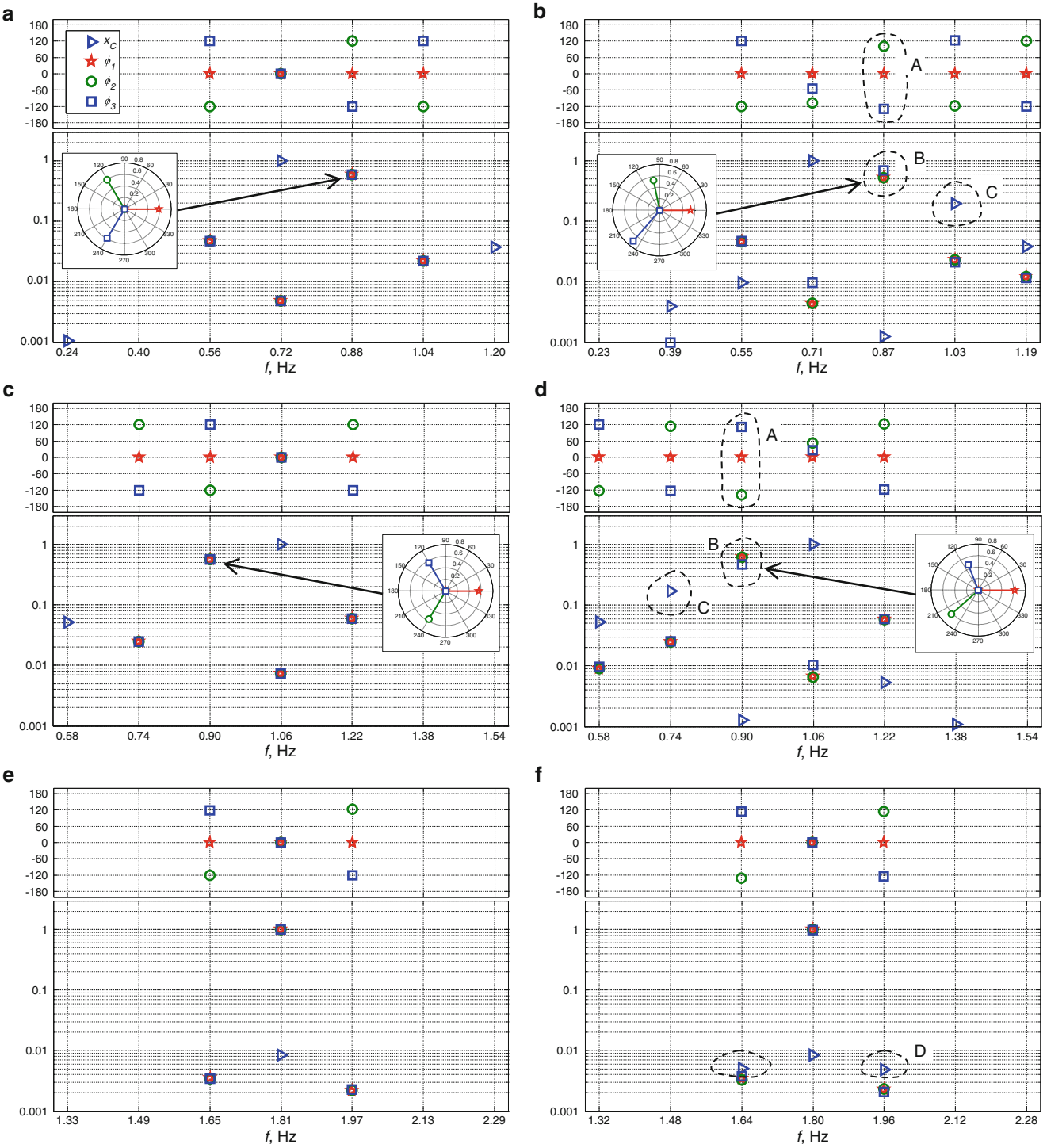

Fig. 14.6 Rotor related modes obtained via Floquet analysis: (**a**, **b**) backward whirling mode, (**c**, **d**) forward whirling mode, (**e**, **f**) collective mode. *Left column*: isotropic rotor in the presence of gravity; *right column*: anisotropic rotor with reduced stiffness of the third blade ($k_c = 0.97k_a$)

The representation of complex Fourier coefficients in Fig. 14.6 may require some explanations. For each mode, the plot shows the magnitude of four DOFs: x_C, ϕ_1, ϕ_2, ϕ_3. The other two DOFs are not shown since their magnitude is much smaller. The magnitude is normalized such a way that the magnitude of the biggest Fourier component is set to unity. The phase subplot shows the phases of the rotor related DOFs ϕ_1, ϕ_2, ϕ_3, which are adjusted such that the phase of ϕ_1 is zero. One has to notice that the plots mix the translational and angular units (for x_C and ϕ_1, ϕ_2, ϕ_3 respectively) thus the direct comparison of the magnitudes corresponding to the different units is not valid.

Comparing the corresponding modes of the isotropic and anisotropic rotors, one can spot some deviations. Naturally, the imaginary parts of the Floquet exponents (namely, the damped natural frequencies, shown by the ticks on the frequency axes) have slightly decreased; this is an obvious result of the reduced rotor stiffness. Secondly, some of the Fourier coefficients describing the mode shapes have changed. One can notice that some Fourier components are affected more than the others. The most evident effects of anisotropy are outlined by a dashed line and labeled by letters A . . . D.

The effects labeled by "A" and "B" represent the significant change of phase and magnitude of blades 1 . . . 3 of the dominant whirling component of the BW and FW modes. This effect is better seen in the complexity plots in the insets. For the BW mode (Fig. 14.6a, b), the magnitude of the blade with the decreased stiffness becomes greater, and the phase between this blade and two other blades becomes greater than 120°. For the FW mode (Fig. 14.6c, d), the effect is opposite: the magnitude of the "damaged" blade becomes smaller and the phase between this blade and two others becomes less than 120°. Generalizing, one can say that the rotor anisotropy causes a *loss of symmetry of the whirling rotor modes*. The idea of using this phenomenon to detect and localize blade damage was introduced and investigated in [16].

The phenomenon labeled by letter C affects both BW and FW modes and appears as a significant increase of side-to-side tower motion at central frequency $\pm 2\Omega$ ("+" for the backward and "−" for the forward mode). Finally, the effect denoted by letter D appears as two sidebands in the tower motion in the collective mode (Fig. 14.6e, f).

Figure 14.7 plots the Fourier coefficients for same three modes, which are now obtained by the H-OMA-TD method applied to the data generated in the simulated experiment. The experiment was repeated five times, every time we generated new random excitation forces; the five datasets containing the simulated dynamic response (each 7200 s long, corresponding to 1150 rotor revolutions) were input to the H-OMA-TD method. The average and confidence intervals of the results are presented in Fig. 14.7. To ease the comparison, we used the same mode normalization and phase rotation scheme as for Fig. 14.6.

As one can see, the abovementioned phenomena due to the rotor anisotropy are caught by the method, though not precisely. The method was able to catch the phase changes due to the anisotropy (the areas denoted by letter A for both backward and forward whirling modes, Fig. 14.7b, d), with quite high confidence. However, the changes in blade magnitudes (areas "B") for these modes are not very evident, though it is present; also, the confidence is lower. The third phenomenon, denoted by letter C is also caught, also with lower confidence. Anyway, it is apparent that the magnitude of the side-to-side component of the whirling modes at the central frequency $\pm 2\Omega$ is about five times higher than for the isotropic rotor. Finally, the method catches the increase of the sidebands magnitudes for the collective mode (areas "D" in Fig. 14.7f), more at 1.64 Hz and less at 1.96 Hz, though again, the confidence is quite low.

It is also clear that the method finds several components that do not exist in the analytical solution (Fig. 14.6). In Fig. 14.7a, they are outlined by the red dashed line and denoted by letter E. These "noise" components all have quite low confidence and can be filtered out. This also points to a challenge in performing this type of identification. The method is prone to identify some component at every line in the spectrum, presumably due to noise or because the input forces are not fully white. Fortunately, the method is most reliable for those response components that contribute most to the motion of the turbine.

It is unclear why the method finds the side-to-side Fourier components at the central frequency $\pm 2\Omega$ in the BW and FW modes for the *isotropic* rotor (outlined by the red dashed line in Fig. 14.7a, c). According to the Floquet analysis, these components should not be present in the modes (see Fig. 14.6a, c). However, the spurious components that were identified in the isotropic case are 5–10× smaller than those in the anisotropic case, so it seems that these components could still be used as a measure of anisotropy.

14.4.2 Application to Data from Simulated Vestas V27 with Introduced Rotor Anisotropy

The simulated experimented conducted on a simple six degree-of-freedom bladed rotor system demonstrated the capabilities of H-OMA-TD to capture the main dynamic effects of rotor anisotropy. However, for the simulations, the rotor was excited by broadband uncorrelated noise, which fulfils OMA assumption regarding the excitation. In reality, the blades of a wind turbine are loaded by aerodynamic forces, which are periodic and partly correlated due to wind turbulence [17]. Wind shear (dependence of the wind speed from the altitude) also causes a strong aerodynamic excitation at 1p. These properties of the excitation can complicate H-OMA-TD, as the loading is not completely fulfil the OMA assumptions.

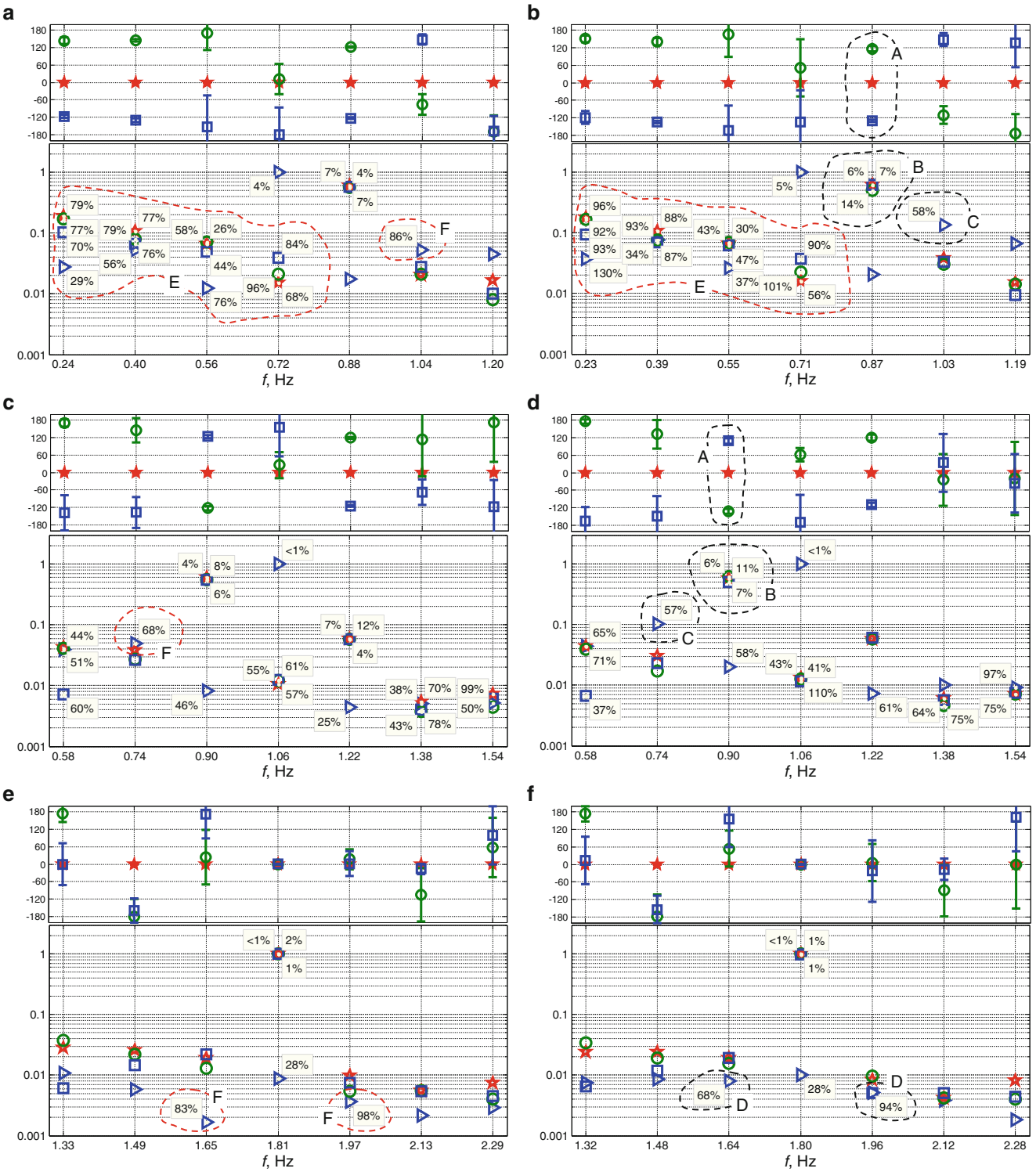

Fig. 14.7 Rotor related modes obtained by H-OMA-TD: (**a**, **b**) backward whirling mode, (**c**, **d**) forward whirling mode, (**e**, **f**) collective mode. *Left column*: isotropic rotor in the presence of gravity; *right column*: anisotropic rotor with reduced stiffness of the third blade ($k_c = 0.97k_a$). The error bars in the phase plots correspond to 95 % confidence; the per-cent values in the magnitude plots denote a half-width 95 % confidence interval as a percentage of the mean magnitude

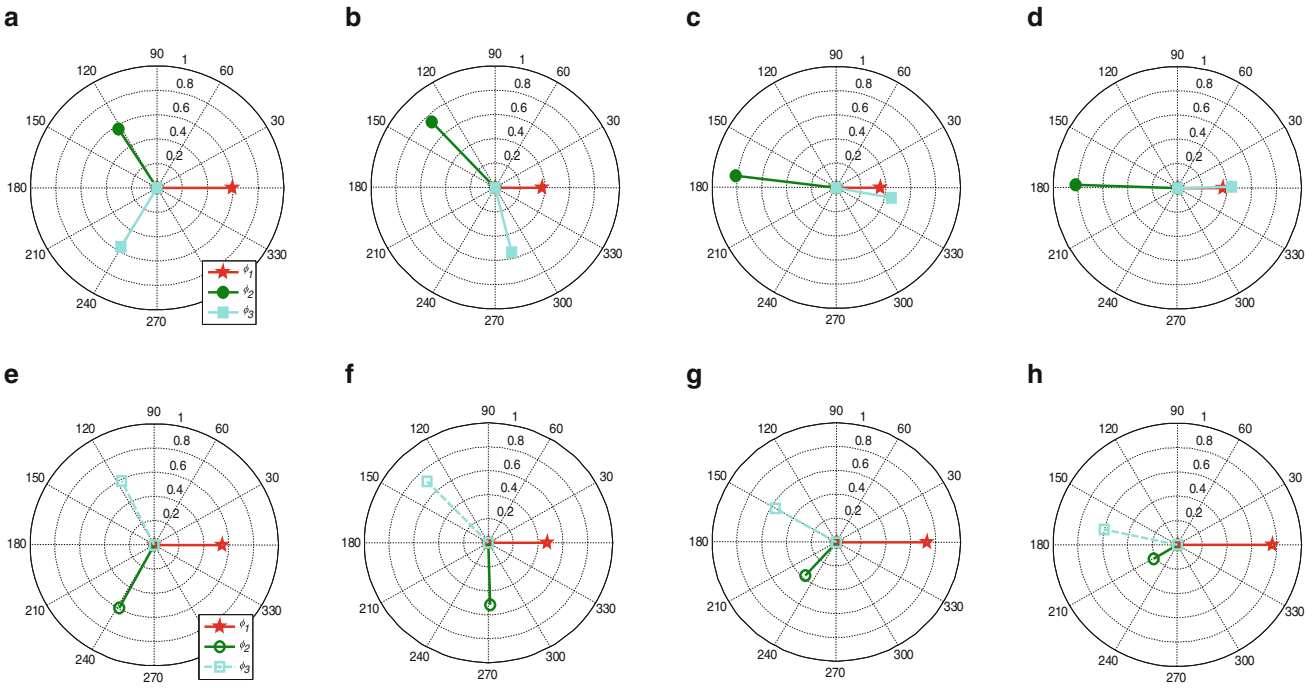

Fig. 14.8 Complexity plots of the dominant components of the whirling modes [16]. *Top*: BW mode: (**a**) isotropic rotor; (**b**) 1 % Young modulus reduction of blade 2; (**c**) 3 % Young modulus reduction of blade 2; (**d**) 5 % Young modulus reduction of blade 2. *Bottom*: FW mode: (**e**) isotropic rotor; (**f**) 1 % Young modulus reduction of blade 2; (**g**) 3 % Young modulus reduction of blade 2; (**h**) 5 % Young modulus reduction of blade 2

In order to check the performance of H-OMA-TD in more realistic scenario, the method was applied to the data generated using *Horizontal Axis Wind turbine Code 2nd generation* (HAWC2). This is a nonlinear aeroelastic code designed for simulation of the wind turbine dynamic response in time domain; the code was developed and maintained by the Wind Energy department of Technical University of Denmark (DTU) [18]. The code models the wind turbulence and calculates the aerodynamic forces acting on the blades. The dynamic response of the blades is simulated employing a multibody formulation, where each blade is represented by an assembly of Timoshenko beam elements.

The vibrations of a Vestas V27 wind turbine were simulated; the same wind turbine type was a test object during the real measurement campaign described later. The detailed description of the modelling, model tuning and setting up a virtual experiment using HAWC2 can be found in [4]. Datasets corresponding to 20 min of wind turbine operating at 32 rpm rotor speed were generated; the rotor anisotropy was modelled by the gradual decrease of Young modulus for blade #2.

Figure 14.8 presents the results of H-OMA-TD applied to the simulated Vestas V27 data. Only the dominant whirling components of the BW and FW modes are shown as complexity plots. Here we see the same tendency as in the insets in Fig. 14.5b, c: for the BW mode, the magnitude of the "damaged" blade becomes greater, while for the FW mode it decreases. The phase between the damaged blade and two others becomes greater than 120° for the BW mode, and oppositely, for the FW mode, it becomes less than 120°. That is, one can see that the H-OMA-TD is able to catch the loss of mode shape symmetry due to the rotor anisotropy but now in more realistic excitation conditions.

14.4.3 Application to Data Measured on Vestas V27 Wind Turbine

This section briefly presents the results of H-OMA-TD applied to the data measured on a real wind turbine (Vestas V27). The details of the measurement setup and the campaign are given in [19].

Starting analyzing data from the real wind turbine, we were not aware about the current rotor state, and we assumed it to be isotropic. In studies [4] and [7], the MBC transformation was applied to the data, and some doubts regarding the rotor isotropy of that particular wind turbine were expressed. Study [9] applied H-OMA-TD to the same data and confirmed the suspected rotor anisotropy. The Fourier coefficients of the BW and FW modes are shown in Fig. 14.9. Both modes are clearly dominated by one component ($m = 0$ corresponds to 3.59 Hz for the BW mode and 3.52 Hz for the FW mode,

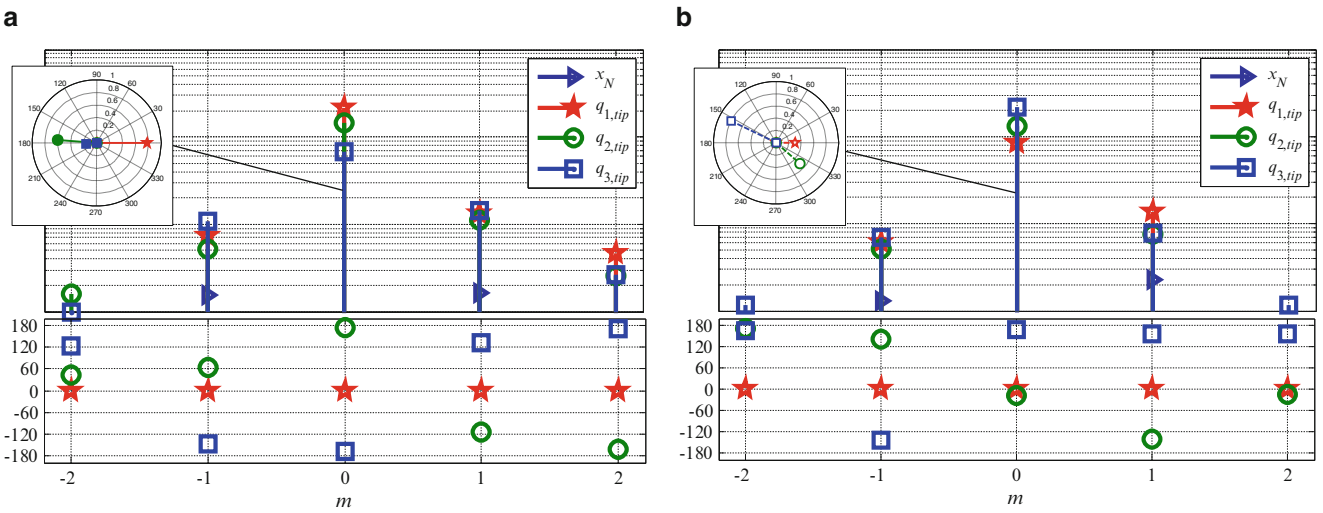

Fig. 14.9 Fourier coefficients: (**a**) BW mode, (**b**) FW mode. *Top*: magnitudes, *bottom*: phase. The *insets* show the complexity plots of the dominant component

for the given case, the rotor speed is 32 rpm).[1] Analyzing the Fourier coefficients of these modes, one can identify some features of the rotor anisotropy, which are listed in Sect. 14.4.1. The mode shapes are not symmetric, all three blades have different magnitudes: the BW mode features the highest magnitude of Blade #1 and lowest of Blade #3, for the FW mode the magnitude order is opposite: Blade #1 is lowest and Blade #3 is highest. The phases do not make a very clear picture; however, one can note almost 180° phase between Blade #1 and two other blades for the BW mode, though the phase distribution of the FW mode does not fit the pattern derived from the analytical model and the simulations.

14.5 Conclusion and Further Research

The paper validates applicability of the time domain implementation of the HPS-based method (referred here as H-OMA-TD) to systems with rotating slightly anisotropic rotor. The validation is based on a simple six DOFs mechanical system resembling a horizontal axis wind turbine and done via comparison with analytic results obtained via Floquet analysis. The method was also applied to data generated via HAWC2 simulations of a Vestas V27 wind turbine and the data measured on a real Vestas V27 machine.

The validation demonstrates that the method can qualitatively catch the important features of rotor anisotropy, such as a loss of symmetry of whirling modes and appearance of the additional side-to-side components in whirling and collective modes. Quantitatively, the method detects some of the effects better than the others, for example, the phase change is detected with good confidence, while the confidence in magnitude change is lower.

Concluding it is important to note that MBC transformation, widely used in wind turbine design, can only produce modes with symmetric mode shapes (see Sect. 14.3.1), thus the MBC-based methods are not capable to catch the abovementioned effects of rotor anisotropy.

Acknowledgement The work was partly supported by EUDP (Danish Energy Technology Development and Demonstration Programme), grant number 64011-0084 “Predictive Structure Health monitoring of Wind Turbines”. The authors wish to acknowledge the great help from Óscar Ramírez Requesón for performing the HAWC2 simulations of the Vestas V27 wind turbine.

[1]Comparing Fig. 14.9 with Figs. 14.6 and 14.7, one has to take into account the scaling between the rotational and translational DOFs: in the analytical and simulation cases, the rotational DOFs are in angular units. In the case of measured data, the rotational DOFs are in translational units (here, the acceleration measured in the tangential direction at the tip of the blades).

References

1. Tcherniak, D., Chauhan, S., Rossetti, M., Font, I., Basurko, J., Salgado, O.: Output-only modal analysis on operating wind turbines: application to simulated data. In: European Wind Energy Conference, Warsaw, Poland (2010)
2. Jhinaoui, A., Mevel, L., Morlier, J.: A new SSI algorithm for LPTV systems: application to a hinged-bladed helicopter. Mech. Syst. Signal Process. **42**(1), 152–166 (2014)
3. Allen, M.S., Sracic, M.W., Chauhan, S., Hansen, M.H.: Output-only modal analysis of linear time-periodic systems with application to wind turbine simulation data. Mech. Syst. Signal Process. **25**, 1174–1191 (2011)
4. Requesón, O.R., Tcherniak, D., Larsen, G.C.: Comparative study of OMA applied to experimental and simulated data from an operating Vestas V27 wind turbine. In: Operational Modal Analysis Conference (IOMAC), Gijón, Spain (2015)
5. Mevel, L., Gueguen, I., Tcherniak, D.: LPTV subspace analysis of wind turbine data. In: European Workshop on Structural Health Monitoring (EWSHM), Nantes, France (2014)
6. Allen, M.S.: Frequency-domain identification of linear time-periodic systems using LTI techniques. J. Comput. Nonlinear Dyn. **4**(4) (2009)
7. Yang, S., Tcherniak, D., Allen, M.S.: Modal analysis of rotating wind turbine using multi-blade coordinate transformation and harmonic power spectrum. In: Int. Modal Analysis Conference (IMAC), Orlando (2014)
8. Tcherniak, D., Yang, S., Allen, M.S.: Experimental characterization of operating bladed rotor using harmonic power spectra and stochastic subspace identification. In: International Conference on Noise and Vibration Engineering (ISMA), Leuven, Belgium (2014)
9. Tcherniak, D., Allen, M.S.: Experimental characterization of an operating Vestas V27 wind turbine using harmonic power spectra and OMA SSI. In: International Operational Modal Analysis Conference (IOMAC), Gijón, Spain (2015)
10. Ewins, D.J.: Modal Testing, Theory, Practice, and Application. Research Study Press, Baldock (2000)
11. Skjoldan, P.F.: Aeroelastic modal dynamics of wind turbines including anisotropic effects. PhD dissertation, Roskilde, Denmark (2011)
12. Hansen, M.H.: Improved modal dynamics of wind turbines to avoid stall-induced vibrations. Wind Energy **6**, 179–195 (2003)
13. Hansen, M.H.: Aeroelastic stability analysis of wind turbines using eigenvalue approach. Wind Energy **7**, 133–143 (2004)
14. Xie, W.-C.: Dynamic Stability of Structures. Cambridge University Press, New York (2006)
15. Wereley, N.M.: Analysis and control of linear periodically time varying systems. PhD dissertation, Department of Aeronautics and Astronautics, Massachusetts Institute of Technology, Cambridge (1991)
16. Tcherniak, D.: Rotor anisotropy as a blade damage indicator for wind turbine structural health monitoring systems. Mech. Syst. Signal Process. (Accepted for publication) (2015)
17. Tcherniak, D., Chauhan, S., Hansen, M.H.: Applicability limits of operational modal analysis to operational wind turbines. In: International Modal Analysis Conference (IMAC), Orlando (2010)
18. Larsen, T.J., Hansen, A.M.: How 2 HAWC2, the User's Manual. Technical University of Denmark, Lyngby (2013)
19. Tcherniak, D., Larsen, G.C.: Application of OMA to an operating wind turbine: now including vibration data from the blade. In: International Operational Modal Analysis Conference (IOMAC), Guimarães, Portugal (2013)